

Perturbative traveling wave solution for a flux limited reaction-diffusion equation of morphogenesis

Waipot Ngamsaad^{a,*}, Suthep Suantai^b

^a*Division of Physics, School of Science, University of Phayao, Phayao 56000, Thailand*

^b*Department of Mathematics, Faculty of Science, Chiang Mai University, Chiang Mai 50200, Thailand*

Abstract

In this paper, we investigate a porous medium-type flux limited reaction-diffusion equation arising in morphogenesis modeling. This nonlinear partial differential equation is an extension of the generalized Fisher-Kolmogorov-Petrovsky-Piskunov (Fisher-KPP) equation in one-dimensional space. The approximate analytical traveling wave solution has been found by using a perturbation method. It reveals that the morphogen concentration propagates as a sharp wavefront where the wave speed has a saturated value. The numerical solutions of this equation have been also provided, in order to compare with the analytical predictions. Finally, we qualitatively compare our theoretical results with the experimental studies.

Keywords: Traveling wave solution, Flux limited Fisher-KPP equation, Morphogenesis

1. Introduction

Reaction-diffusion models, formulated by the nonlinear partial differential equations, have a wide range of applications in physics, chemistry and biology (see Ref. [1] for review). The most recognized reaction-diffusion model is the Fisher-Kolmogorov-Petrovsky-Piskunov (Fisher-KPP) equation whose solution demonstrates the traveling wave propagation that switch between equilibrium states [2, 3]. Inspired by these seminal works, finding the traveling wave solutions of the reaction-diffusion equations has been attractive—since it provides insight into the underlying physical dynamics in the natural processes.

In developmental biology, it has been hypothesized that the concentration gradient of secreted signaling molecules, known as *morphogens*, regulate structure and pattern formation of the tissues [4–7]. Reaction-diffusion equations have been employed as models of morphogenesis [8–10] since the pioneer works

*Corresponding author

Email addresses: waipot.ng@up.ac.th (Waipot Ngamsaad), suthep.s@cmu.ac.th (Suthep Suantai)

of Turing [11], Crick [12], Gierer and Meinhardt [13]. However, the classical theory describes the migration of morphogens as linear diffusion or random-walk motion in microscopic point of view [8, 10–13]. Unfortunately, the experimental results of some specific morphogens, such as Hedgehog (Hh) molecules, show that the classical reaction-diffusion equations are unable to capture the realistic morphogenetic patterns [14, 15]. The model based on the linear diffusion [9] reproduces unclear front which conflicts with the experimental observations [14, 15]. In addition, the classical diffusion models has shortcoming—it contains the infinite flux with concentration gradient [16]. To remedy unphysical issues, the authors in Refs. [14, 15] proposed the flux limited reaction-diffusion equations as the model of morphogen transport. It seems likely that this novel model results more realistic morphogenetic pattern—which is verified by the experimental the data [14, 15].

The flux limited diffusion equation can be derived from two different approaches, including the special relativistic-like mechanics [16] and the the optimal transport theory [17]. Later, it has been extended to the flux limited porous medium-type diffusion equation for the generalization [18, 19]. Combining with reaction processes, the flux limited reaction-diffusion equations have been studied by many authors [20–29]. As exemplified by the propagation of Sonic Hedgehog (Shh) molecules in a neural tube along the dorsal-ventral axis, the one-dimensional model is plausible for the real morphogenetic system [14, 15].

Motivated by this biological system, in this paper, we investigate a one-dimensional porous medium-type flux limited reaction-diffusion equation as a simplified model of morphogenesis. Although the variance of the flux limited reaction-diffusion models have been studied in published literatures so far [20, 21, 24, 25, 27, 30], to the best of our knowledge, the exact solutions are currently unsolvable. Therefore, the objective of this research is to find the approximate analytical traveling wave solution of this equation by using a simple perturbation method, as used in the previous works [31, 32]. This simple approximation approach is similar to an asymptotic analysis [1]; and it uncovers two main physical features, including morphogen concentration profile and the propagating speed of wavefront. To obtain its solution in the precise value, we also solve this equation by using a robust fully implicit numerical scheme. Finally, we qualitatively compare our solutions with the published experimental evidences. We hope that our solutions could provide insight into the spreading and the pattern formation of morphogenesis modeled by this simple flux limited reaction-diffusion process.

2. Model description

The one-dimensional porous medium-type flux limited reaction-diffusion equation in our consideration has been presented in Ref [25] which is given by

$$\rho_t = \mu \left(\frac{\rho \rho_x}{\sqrt{1 + \frac{\mu^2}{c_s^2} \rho_x^2}} \right)_x + R(\rho), \quad (1)$$

where $\rho(x, t)$ is morphogen concentration at position x and time t , μ is viscosity constant, c_s is speed of sound and $R(\rho)$ is reaction term [25]. For the sake of simplicity, similar to Refs. [21, 24, 25, 27], the choice for reaction term is the logistic law

$$R(\rho) = \alpha\rho \left(1 - \frac{\rho}{\rho_m}\right), \quad (2)$$

where α is rate constant and ρ_m is the maximum concentration. To see the physical meaning of the viscosity constant, we define $\mu = c_s^2/(\gamma\rho_m)$ where γ is frictional rate. From Eq. (1) without reaction term, when the value of γ is small the diffusion is fast and when the value γ is large the diffusion is slow. We rewrite Eq. (1) in the general form of reaction-diffusion equation $u_t = -j_x + f(\rho)$ where $j(x, t)$ is the flux defined by $j(x, t) = \rho(x, t)V(x, t)$ and $V(x, t)$ is the velocity field. Therefore, from Eq. (1), the velocity field is given by

$$V = -\mu \frac{\rho_x}{\sqrt{1 + \frac{\mu^2}{c_s^2} \rho_x^2}}. \quad (3)$$

For convenience in further analysis, we introduce the dimensionless quantities as follows: $u = \rho/\rho_m$, $t' = \alpha t$ and $\epsilon = \alpha/\gamma$. Due to the constraint that c_s is the highest admissible speed, we choose the dimensionless velocity as $v = V/c_s$. According to $dx' \sim v dt'$, the dimensionless position is provided by $x' = (\alpha/c_s)x$. Now the dimensionless concentration and velocity are limited such that $0 \leq u \leq 1$ and $0 \leq |v| \leq 1$, respectively. Substituting Eq. (2) into Eq. (1) with all defined dimensionless quantities, we obtain the flux limited reaction-diffusion equation in dimensionless form

$$u_t = \left(\frac{\epsilon u u_x}{\sqrt{1 + \epsilon^2 u_x^2}} \right)_x + u(1 - u), \quad (4)$$

where prime symbols have dropped. Similarly for Eq. (3), the dimensionless velocity field is given by

$$v = -\frac{\epsilon u_x}{\sqrt{1 + \epsilon^2 u_x^2}}. \quad (5)$$

Eq. (4) is exactly the generalized Fisher-Kolmogorov-Petrovsky-Piskunov (Fisher-KPP) equation [33] with the flux limited diffusion extension. It is *degenerate* at $u = 0$ that it transforms from the second-order to the first-order differential equation. It well understood that the degenerate reaction-diffusion equation results a clear wavefront interface, providing that the concentration profile vanishes at a finite position [1, 33]. This feature can be observed in the experimental results of morphogenesis [14, 15]. There appears only one parameter in our system that is the ratio of reaction rate to the frictional rate ϵ . It has a crucial role on the regulation of this system. When $\epsilon \rightarrow 0$, Eq. (4) recovers a logistic reaction equation, $u_t = u(1 - u)$, which has no propagating front. As $\epsilon \rightarrow \infty$, it converges to a reaction-convection equation, $u_t \approx (u u_x / |u_x|)_x + u(1 - u)$, whose solution propagates with the saturated speed $c = 1$ (or c_s in physical

unit). Therefore, it promises that the flux limited reaction-diffusion equation eliminates the shortcoming in infinite propagating speed for all range of parameter or even large concentration gradient [21, 24, 27]. With these features, the flux limited model is more realistic than the classical theory for description of the biological transport processes.

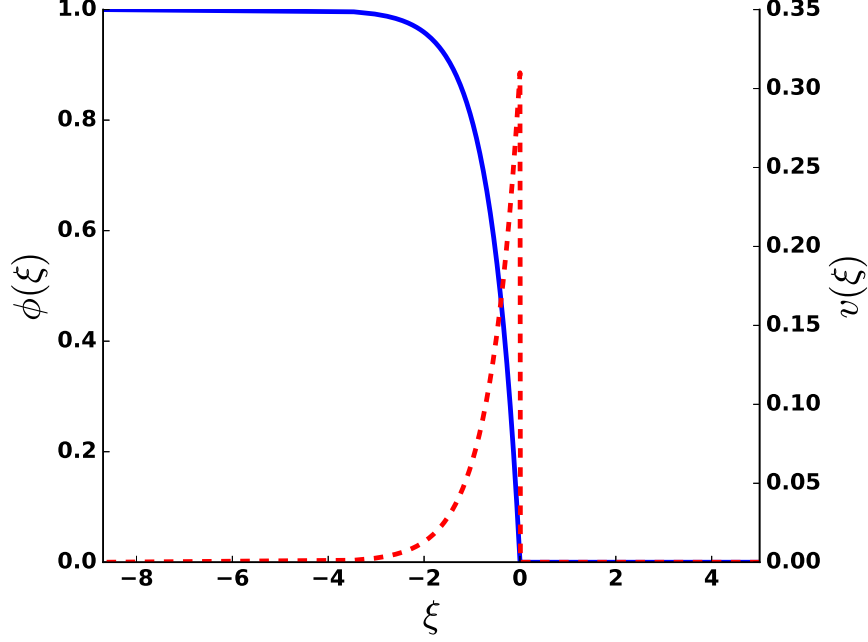


Figure 1: (Color online) The plot of the analytical wave profile Eq. (20) (straight line) and the corresponding velocity field Eq. (19) (dashed line) for $\epsilon = 0.2$.

3. Perturbative traveling wave solution

We now assume that the solution of Eq. (4) is in the traveling wave form $u(x, t) = \phi(\xi)$ where $\xi = x - ct$ and c is front speed. Substituting this solution into Eq. (4) and Eq. (5), respectively, we obtain

$$\left(\frac{\epsilon \phi \phi_\xi}{\sqrt{1 + \epsilon^2 \phi_\xi^2}} \right)_\xi + c \phi_\xi + \phi (1 - \phi) = 0, \quad (6)$$

and

$$v(\xi) = - \frac{\epsilon \phi_\xi}{\sqrt{1 + \epsilon^2 \phi_\xi^2}}. \quad (7)$$

For simplicity, we define the rescaled variables, $z = \xi/\sqrt{\epsilon}$ and $\nu = c/\sqrt{\epsilon}$, that Eq. (4) reads

$$\left(\frac{\phi\phi_z}{\sqrt{1+\epsilon\phi_z^2}} \right)_z + \nu\phi_z + \phi(1-\phi) = 0. \quad (8)$$

Eq. (8) is the main equation that we attend to analyze in this research. Solving for the exact solution of Eq. (8) in general case is not yet available thus we are interested in a special case where $\epsilon \ll 1$. This can happen when either the growth rate is slow, $\alpha \rightarrow 0$, or the frictional rate is high, $\gamma \rightarrow \infty$.

Here, we employ a simple perturbation method for finding the solution of Eq. (8) as presented in published literatures [1, 31, 32]. By using the Taylor expansion, Eq. (8) can be written in approximate form

$$\left[\phi \left(\phi_z - \frac{\epsilon}{2} \phi^3 \right) \right]_z + \nu\phi_z + \phi(1-\phi) + O(\epsilon^2) = 0. \quad (9)$$

Next, we define $\phi_z = w(\phi)$ and then we rewrite Eq. (9)

$$\phi \left(w - \frac{3\epsilon}{2} w^3 \right) w' - \frac{\epsilon}{2} w^4 + w^2 + \nu w + \phi(1-\phi) = 0, \quad (10)$$

where $(*)' \equiv d(*)/d\phi$. The solution of Eq. (10) can be written in the power series of ϵ (up to the first order)

$$w(\phi) = w_0(\phi) + w_1(\phi)\epsilon + O(\epsilon^2), \quad (11)$$

$$\nu = c_0 + c_1\epsilon + O(\epsilon^2), \quad (12)$$

where w_* and c_* , respectively, are undetermined concentration wave gradients and wave speeds. Substituting Eq. (11) and Eq. (12) into Eq. (10), we have

$$\begin{aligned} & \phi \left(w_0 w'_0 + w'_0 w_1 \epsilon + w_0 w'_1 \epsilon - \frac{3}{2} w_0^3 w'_0 \epsilon \right) \\ & - \frac{1}{2} w_0^4 \epsilon + w_0^2 + 2w_0 w_1 \epsilon + c_0 w_0 + c_1 w_0 \epsilon + c_0 w_1 \epsilon \\ & + \phi(1-\phi) + O(\epsilon^2) = 0. \end{aligned} \quad (13)$$

Comparing the coefficients of the ϵ^0 and ϵ^1 terms, respectively, we obtain

$$\phi w_0 w'_0 + w_0^2 + c_0 w_0 + \phi(1-\phi) = 0 \quad (14)$$

and

$$\begin{aligned} & \phi w_0 w'_1 + (\phi w'_0 + 2w_0 + c_0) w_1 \\ & - \frac{3}{2} \phi w_0^3 w'_0 - \frac{1}{2} w_0^4 + c_1 w_0 = 0. \end{aligned} \quad (15)$$

Eq. (14) has the known solutions in the published literatures [1, 33], given by

$$w_0(\phi) = \frac{1}{\sqrt{2}}(\phi - 1), \quad c_0 = \frac{1}{\sqrt{2}}. \quad (16)$$

Using Eq. (16), Eq. (15) can be solved as shown in the Appendix A. Gathering all terms, finally, we have the approximate solutions (up to the first-order correction)

$$w(\phi) = \frac{1}{\sqrt{2}} (\phi - 1) \left[1 + \frac{\epsilon}{6} \left(\phi^2 - \frac{21}{10} \phi + \frac{6}{5} \right) \right], \quad (17)$$

$$\nu = \frac{1}{\sqrt{2}} \left(1 - \frac{\epsilon}{20} \right). \quad (18)$$

Using the transformation $\phi_\xi = \phi_z / \sqrt{\epsilon} = w / \sqrt{\epsilon}$, from Eq. (7), we found the solution for the velocity field

$$v(\phi(\xi)) = - \frac{\sqrt{\epsilon} w(\phi(\xi))}{\sqrt{1 + \epsilon w^2(\phi(\xi))}}. \quad (19)$$

And, from Eq. (17), after evaluating the integral $\sqrt{\epsilon} \int d\phi / w(\phi) = \int d\xi$, we found the approximate analytical solution for the wave profile

$$a \ln \frac{(\phi - 1)^2}{1 + \frac{\epsilon}{6} \left(\phi^2 - \frac{21}{10} \phi + \frac{6}{5} \right)} + 2ab \tan^{-1} b (20\phi - 21) + \xi_0 = \xi, \quad (20)$$

where $a = \frac{30\sqrt{2}\epsilon}{60+\epsilon}$, $b = \frac{\sqrt{\epsilon}}{\sqrt{2400+39\epsilon}}$ and $\xi_0 = a [\ln(1 + \frac{\epsilon}{5}) + 2b \tan^{-1} 21b]$, determined by using the boundary condition $\phi(0) = 0$. Although Eq. (20) is implicit solution, the variables are separated explicitly; so we can plot the wave profile and the corresponding velocity field Eq. (19) as demonstrated in Fig. (1). Noticing that, the solutions in Eq. (17), Eq. (19) and Eq. (20) are available for $0 \leq \phi \leq 1$, otherwise they are zero. The wave profiles have the sharp front interface where the concentration falls to zero at a finite front position. This feature is in qualitative agreement with the experimental observation where the morphogen concentration profiles have a clear invading front interface [14, 15].

To obtain the better approximate wave speed function, we use the fact that the front speed is the velocity field at the leading edge $c = v(0)$. So that, from Eq. (17) and Eq. (19), we have

$$c(\epsilon) = \sqrt{\frac{\epsilon}{2}} \frac{1 + \epsilon/5}{\sqrt{1 + \frac{\epsilon}{2} (1 + \epsilon/5)^2}}. \quad (21)$$

Expanding Eq. (21), it proves that $c/\sqrt{\epsilon} \approx (1 - \frac{\epsilon}{20})/\sqrt{2} + O(\epsilon^2) = \nu$ which is consistence with the first order approximate solution in Eq. (18). As $\epsilon \rightarrow \infty$, from Eq. (21), the wave speed reaches the limited value at $c = 1$ (or c_s in physical unit). It proves that this flux limited reaction-diffusion equation promises the saturated wave speed as required for biological applications [14, 15].

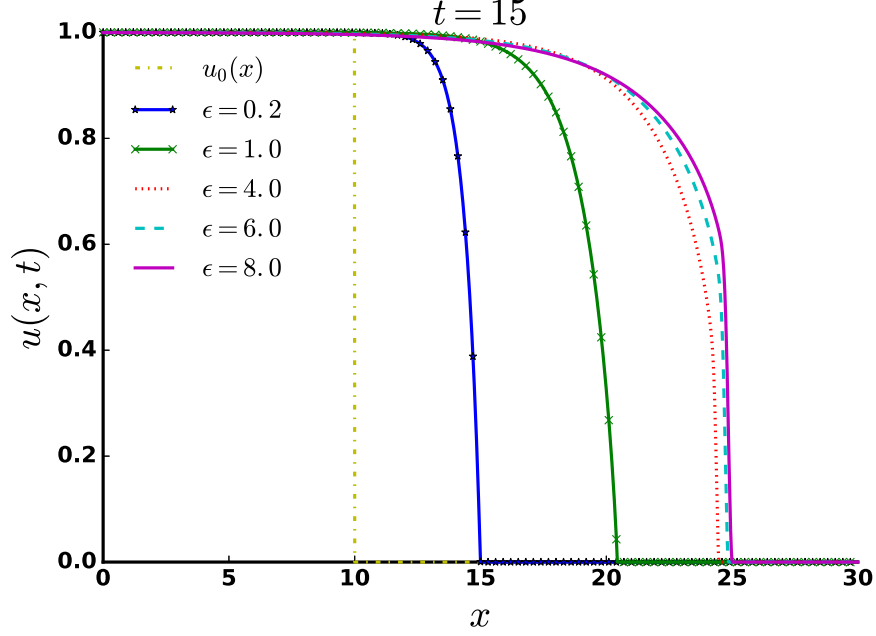


Figure 2: (Color online) The numerical concentration profiles at $t = 15$ for some selected values of the rate ratio ϵ . The dashdot line represents the initial profile.

4. Numerical solutions and discussion

In order to compare the analytical predictions with more accurate numerical values, we solved the dimensionless flux limited reaction-diffusion equation (Eq. (4)) by using a nonstandard fully implicit finite-difference method [32, 34]. First of all, we rewrite Eq. (4) in the usual form of reaction-diffusion equation

$$u_t = [M(u, u_x)u_x]_x + f(u)u, \quad (22)$$

where $M(u, u_x) = \epsilon u / \sqrt{1 + \epsilon^2 u_x^2}$ which is equivalent to the nonlinear diffusion coefficient and $f(u) = 1 - u$ acts as nonlinear reaction rate. It is known that solving Eq. (22) with a standard explicit method is inefficiency due to the variable diffusion coefficient [35]. Thus, solving with a standard implicit scheme is even harder due to nonlinearity of equation. The idea of nonstandard fully implicit finite-difference method is that only linear terms are discretized forward in time. Then, to do so, we define the discrete space and time as follows: $x_i = i\delta x$, $t_n = n\delta t$, where δx is a grid spacing, δt is a time step, $i \in \{0, 1, 2, \dots, J\}$, $n \in \{0, 1, 2, \dots, N\}$, and J and N are integers. Now, the discrete concentration reads $u_i^n = u(x_i, t_n)$. So that, Eq. (22) in discrete form is provided by

$$\frac{\partial}{\partial t} u_i^{n+1} \approx \frac{\partial}{\partial x} \left(M_i^n \frac{\partial}{\partial x} u_i^{n+1} \right) + f_i^n u_i^{n+1}, \quad (23)$$

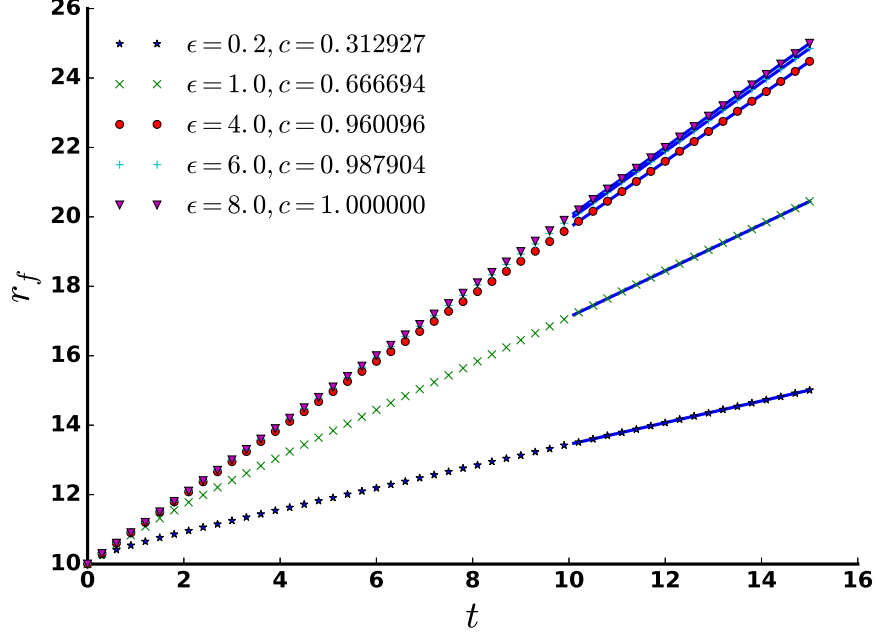


Figure 3: (Color online) The front position versus time, corresponded to the concentration profiles in Fig. (2). The markers show for every 3 data points. The solid lines represent the linear fitting curve for the last 50 data.

where $M_i^n = M(u_i^n, \partial u_i^n / \partial x)$ and $f_i^n = 1 - u_i^n$. By using this approach, Eq. (23) can be evaluated to the tridiagonal matrix equation as usual. This numerical scheme has proven stable enough for solving this sort of nonlinear partial differential equation. The complete evaluation of algorithm and stability analysis are described in the Appendix B.

In our computations, we chose the grid spacing and the time step, respectively, as follows: $\delta x = 0.01$ and $\delta t = 0.01$. All calculations were performed on 3,000 grids with 1,500 iterations that cover spatial length 30 and total time 15 in dimensionless units. The initial concentration profile, $u_0(x)$, was set to a step function:

$$u_0(x) = \begin{cases} 1, & x < 10 \\ 0, & x \geq 10. \end{cases} \quad (24)$$

The zero flux condition, $u_x = 0$, was imposed at the boundaries. The demonstration of the concentration profiles by varying the rate ratio (ϵ), obtained from the numerical method, are shown in Fig. (2). It found that the concentration profiles evolve with the sharp traveling wave that falls to zero at a finite front position r_f , as predicted in the analytical solution. The the wave profile has more smoother interface as the value of ϵ increases. This is due to the frictional rate γ is small relatively to the growth rate α so that the morphogens migrate

toward the free space faster. For the large values of ϵ , the profiles in equal time trend to overlap which shows that the front speed trends to reach a saturated value.

To compute the wave speed, the front positions were collected for every $t = 0.1$. Due to numerical deviation, the front position was determined by the first position where the concentration was lower than 1×10^{-6} . The last 50 data points were selected for fitting with the linear equation, $r_f = ct + r_0$, so that the wave speed is the slope of the fitted equation. The plots of corresponding front position versus time are shown in Fig. (3). Our numerical front positions were fitted well with the linear equation, indicating that the concentration propagates with constant front speed.

The plot of the numerical front speed c versus the rate ratio ϵ , as compared with the analytical predication in Eq. (21), is shown in Fig. (4). We found in both analytical and numerical data that the front speed increases with ϵ . It reaches the saturated value, at $c = 1$, as ϵ approaches a large value. The analytical result agrees well with the numerical data for the small value of rate ratio ($\epsilon \ll 1$), since the correction of our analytical solution was only $O(\epsilon^2)$.

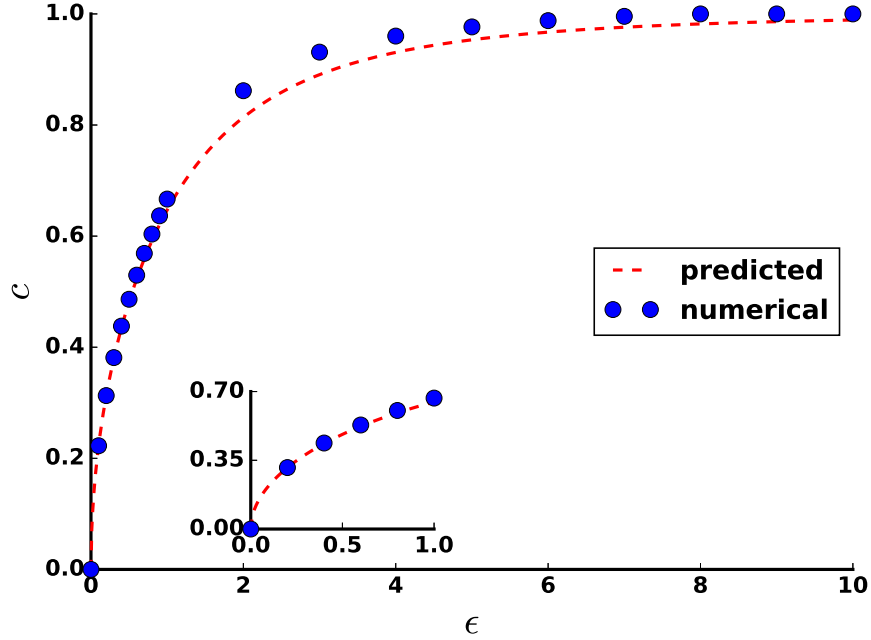


Figure 4: (Color online) The front speed versus the rate ratio ϵ . The circle markers represent the numerical results and the dash lines represent the predicted front speed from Eq. (21). The inset shows the data for small values of ϵ .

To this end, our solutions to this simple flux limited reaction-diffusion equation, both analytical and numerical, capture some physical features of morpho-

genesis. Saying that, the wave profiles have a sharp front interface where the concentration falls to zero at a finite front position. This feature is in qualitative agreement with the experimental observations where the morphogen concentration profiles have a clear invading front interface [14, 15]. Finally, it proves that this flux limited reaction-diffusion equation promises the saturated wave speed—which is more realistic model against the conventional theory [16].

5. Conclusions

In summary, we studied a simplified morphogenesis model which is governed by a porous medium-type flux limited reaction-diffusion equation. This equation is actually an extension of the generalized Fisher-KPP equation. The approximate analytical solutions of this equation were admissible by using a perturbation approach. We also solved this equation by using a nonstandard fully implicit finite-difference method, in order to compare with the analytical predictions. It showed that the morphogen concentration propagates as a sharp traveling wave which vanishes at a finite front position. It reproduces clear front interface. The front speed increases as the ratio of the growth rate to the frictional rate increases and reaches the saturated value for the larger value of this rate ratio. One shows that the flux limited reaction-diffusion model eliminates the shortcoming of the classical models—that provide the unphysical infinite front speed. These features are in qualitative agreement with the experimental observations.

Acknowledgment

This research was supported by Research Fund for DPST Graduate with First Placement (*Grant no.* 28/2557) funded by The Institute for the Promotion of Teaching Science and Technology (IPST).

Appendix A. Evaluation of $w_1(\phi)$ and c_1

Substituting Eq. (16) into Eq. (15), we have

$$\begin{aligned} & \phi(\phi - 1)w_1' + (3\phi - 1)w_1 \\ & + \left[c_1 - \frac{1}{4\sqrt{2}}(4\phi - 1)(\phi - 1)^2 \right](\phi - 1) = 0. \end{aligned} \quad (\text{A.1})$$

Eq. (A.1) is a linear first-order ordinary differential equation of the form

$$w_1' + p(\phi)w_1 = q(\phi), \quad (\text{A.2})$$

where $p(\phi) = (3\phi - 1)/[\phi(\phi - 1)]$ and $q(\phi) = \frac{1}{4\sqrt{2}}(4\phi - 1)(\phi - 1)^2/\phi - c_1/\phi$. The solution of Eq. (A.2) is given by $w_1 = (C + \int I(\phi)q(\phi)d\phi)/I(\phi)$ where

$I(\phi) = e^{\int p(\phi) d\phi}$, called integrating factor, and C is integral constant [36]. After evaluating, we found $I = \phi(\phi - 1)^2$ and then we have

$$w_1(\phi) = \frac{1}{\phi(\phi - 1)^2} \left\{ C + (\phi - 1)^3 \times \left[\frac{1}{6\sqrt{2}} (\phi - 1)^2 \left(\phi - \frac{1}{10} \right) - \frac{c_1}{3} \right] \right\}. \quad (\text{A.3})$$

To remove singularities at $\phi = 0$ and $\phi = 1$, it is required that $C = 0$ and $c_1 = -\frac{1}{20\sqrt{2}}$. So that, the first-order concentration wave gradient is provided by

$$w_1(\phi) = \frac{1}{6\sqrt{2}} (\phi - 1) \left(\phi^2 - \frac{21}{10}\phi + \frac{6}{5} \right). \quad (\text{A.4})$$

Appendix B. Evaluation of numerical scheme and stability analysis

The differential operators in Eq. (23) are discretized further [32, 34], then we obtain

$$\begin{aligned} \frac{u_i^{n+1} - u_i^n}{\delta t} &= \frac{1}{(\delta x)^2} \left[M_{i+1/2}^n (u_{i+1}^{n+1} - u_i^{n+1}) \right. \\ &\quad \left. - M_{i-1/2}^n (u_i^{n+1} - u_{i-1}^{n+1}) \right] + f_i^n u_i^{n+1}, \end{aligned} \quad (\text{B.1})$$

where

$$M_{i-1/2}^n = M\left(\frac{u_{i-1}^n + u_i^n}{2}, \frac{u_i^n - u_{i-1}^n}{\delta x}\right), \quad (\text{B.2})$$

$$M_{i+1/2}^n = M\left(\frac{u_i^n + u_{i+1}^n}{2}, \frac{u_{i+1}^n - u_i^n}{\delta x}\right). \quad (\text{B.3})$$

Noting that the correction of Eq. (B.1) is $O(\delta t, (\delta x)^2)$. After rearranging Eq. (B.1), we have

$$\alpha_i^n u_{i-1}^{n+1} + \theta_i^n u_i^{n+1} + \beta_i^n u_{i+1}^{n+1} = u_i^n, \quad (\text{B.4})$$

where

$$\begin{aligned} \alpha_i^n &= -\mu M_{i-1/2}^n, \\ \beta_i^n &= -\mu M_{i+1/2}^n, \\ \theta_i^n &= 1 - \delta t f_i^n + \mu \left(M_{i-1/2}^n + M_{i+1/2}^n \right), \\ \mu &= \delta t / (\delta x)^2. \end{aligned} \quad (\text{B.5})$$

By imposing the zero-flux condition at the boundary grid Ω , saying $u_x|_{\Omega} \approx \frac{u_{\Omega+1}^n - u_{\Omega-1}^n}{2\delta x} + O((\delta x)^2) = 0$, it found that $u_{\Omega-1}^n = u_{\Omega+1}^n$ and $M_{\Omega-1/2}^n = M_{\Omega+1/2}^n$. According to the boundary condition, we have $\beta_0^n = -2\mu M_{1/2}^n$, $\alpha_J^n = -2\mu M_{J-1/2}^n$, $\theta_0^n = 1 - \delta t f_0^n + 2\mu M_{1/2}^n$ and $\theta_J^n = 1 - \delta t f_J^n + 2\mu M_{J-1/2}^n$. Eq. (B.4) can be written

in a tridiagonal matrix equation which can be solved numerically at each time step to obtain the numerical concentration profile u_i^n [32, 35]. The tridiagonal matrix equation is given by

$$\mathbf{A}^n \cdot \mathbf{U}^{n+1} = \mathbf{U}^n, \quad (\text{B.6})$$

where

$$\mathbf{A}^n = \begin{bmatrix} \theta_0^n & \beta_0^n & \cdots & \cdots & 0 \\ \alpha_1^n & \theta_1^n & \beta_1^n & & \vdots \\ \vdots & \ddots & \ddots & \ddots & \vdots \\ \vdots & & \alpha_{J-1}^n & \theta_{J-1}^n & \beta_{J-1}^n \\ 0 & \cdots & \cdots & \alpha_J^n & \theta_J^n \end{bmatrix}, \quad (\text{B.7})$$

and

$$\mathbf{U}^n = [u_0^n \ u_1^n \ u_2^n \ \cdots \ u_J^n]^T. \quad (\text{B.8})$$

We analyze the stability of this numerical scheme (Eq. (B.4)) by using the von Neumann approach that assumes

$$u_i^n = (\lambda)^n e^{\mathbf{i}k i \delta x}, \quad (\text{B.9})$$

where $\mathbf{i} = \sqrt{-1}$, λ represents the amplification factor and k is the wave number [35]. Substituting Eq. (B.9) into Eq. (B.1), we have $\lambda^{-1} = 1 - \delta t f_i^n - \mu M_{i+1/2}^n (e^{\mathbf{i}k \delta x} - 1) + \mu M_{i-1/2}^n (1 - e^{-\mathbf{i}k \delta x})$ which can be approximated further to obtain

$$\lambda \approx [1 - \delta t f_i^n + 4\mu M_i^n \sin^2(k \delta x/2) + O(\delta x)]^{-1}. \quad (\text{B.10})$$

As u_i^n grows from 0 to 1, we have that $0 \leq f_i^n \leq 1$ and $0 \leq M_i^n < \infty$. At the saturated concentration $f_i^n(u_i^n = 1) = 0$, it guarantees $0 < \lambda < 1$. Based on Eq. (B.9) and Eq. (B.10), the numerical solution could converge to a finite value, as long as $\delta x \ll 1$ and $\delta t \ll 1$. Therefore, this algorithm is stable enough for solving this type of nonlinear partial differential equation [32, 34].

References

- [1] Murray J. Mathematical Biology. Springer-Verlag, New York; 1989.
- [2] Fisher R. The wave of advance of advantageous genes. *Ann Eugenics* 1937;7(4):355–69.
- [3] Kolmogorov A, Petrovskii I, Piscounov N. A study of the diffusion equation with increase in the amount of substance, and its application to a biological problem. In: Tikhomirov V, editor. *Selected works of AN Kolmogorov*. Springer; 1991, p. 242–70.
- [4] Dessaud E, Yang LL, Hill K, Cox B, Ulloa F, Ribeiro A, et al. Interpretation of the sonic hedgehog morphogen gradient by a temporal adaptation mechanism. *Nature* 2007;450(7170):717.

- [5] Rogers KW, Schier AF. Morphogen gradients: From generation to interpretation. *Annu Rev Cell Dev Biol* 2011;27(1):377–407. doi:10.1146/annurev-cellbio-092910-154148; pMID: 21801015.
- [6] Briscoe J, Théron PP. The mechanisms of hedgehog signalling and its roles in development and disease. *Nat Rev Mol Cell Biol* 2013;14(7):416.
- [7] Simon E, Aguirre-Tamaral A, Aguilar G, Guerrero I. Perspectives on intra- and intercellular trafficking of hedgehog for tissue patterning. *J Dev Biol* 2016;4(4). URL: <http://www.mdpi.com/2221-3759/4/4/34>. doi:10.3390/jdb4040034.
- [8] Lander AD, Nie Q, Wan FY. Do morphogen gradients arise by diffusion? *Dev Cell* 2002;2(6):785–96. URL: <http://www.sciencedirect.com/science/article/pii/S153458070200179X>. doi:[https://doi.org/10.1016/S1534-5807\(02\)00179-X](https://doi.org/10.1016/S1534-5807(02)00179-X).
- [9] Saha K, Schaffer DV. Signal dynamics in sonic hedgehog tissue patterning. *Development* 2006;133(5):889–900.
- [10] Kondo S, Miura T. Reaction-diffusion model as a framework for understanding biological pattern formation. *Science* 2010;329(5999):1616–20. URL: <https://science.sciencemag.org/content/329/5999/1616>. doi:10.1126/science.1179047.
- [11] Turing AM. The chemical basis of morphogenesis. *Phil Trans Roy Soc B* 1952;237:37.
- [12] Crick F. Diffusion in embryogenesis. *Nature* 1970;225(5231):420.
- [13] Gierer A, Meinhardt H. A theory of biological pattern formation. *Kybernetik* 1972;12(1):30–9. URL: <https://doi.org/10.1007/BF00289234>. doi:10.1007/BF00289234.
- [14] Verbeni M, Snchez O, Mollica E, Siegl-Cachedenier I, Carleton A, Guerrero I, et al. Morphogenetic action through flux-limited spreading. *Phys Life Rev* 2013;10(4):457–75. URL: <http://www.sciencedirect.com/science/article/pii/S1571064513000833>. doi:<https://doi.org/10.1016/j.plrev.2013.06.004>.
- [15] Sánchez Ó, Calvo J, Ibáñez C, Guerrero I, Soler J. Modeling hedgehog signaling through flux-saturated mechanisms. In: *Hedgehog signaling protocols*. Springer; 2015, p. 19–33.
- [16] Rosenau P. Tempered diffusion: A transport process with propagating fronts and inertial delay. *Phys Rev A* 1992;46:R7371–4. URL: <https://link.aps.org/doi/10.1103/PhysRevA.46.R7371>. doi:10.1103/PhysRevA.46.R7371.

- [17] Brenier Y. Extended monge-kantorovich theory. In: Optimal transportation and applications. Springer; 2003, p. 91–121.
- [18] Chertock A, Kurganov A, Rosenau P. Formation of discontinuities in flux-saturated degenerate parabolic equations. *Nonlinearity* 2003;16(6):1875. URL: <http://stacks.iop.org/0951-7715/16/i=6/a=301>.
- [19] Caselles V, et al. Flux limited generalized porous media diffusion equations. *Publicacions Matemàtiques* 2013;57(1):144–217.
- [20] Kurganov A, Rosenau P. On reaction processes with saturating diffusion. *Nonlinearity* 2006;19(1):171. URL: <http://stacks.iop.org/0951-7715/19/i=1/a=009>.
- [21] Andreu F, Caselles V, Mazn J. A fisherkolmogorov equation with finite speed of propagation. *J Differ Equations* 2010;248(10):2528 –61. URL: <http://www.sciencedirect.com/science/article/pii/S0022039610000124>. doi:<https://doi.org/10.1016/j.jde.2010.01.005>.
- [22] Andreu F, Calvo J, Mazn J, Soler J. On a nonlinear flux-limited equation arising in the transport of morphogens. *J Differ Equations* 2012;252(10):5763 –813. URL: <http://www.sciencedirect.com/science/article/pii/S0022039612000411>. doi:<https://doi.org/10.1016/j.jde.2012.01.017>.
- [23] Garrione M, Sanchez L. Monotone traveling waves for reaction-diffusion equations involving the curvature operator. *Bound Value Probl* 2015;2015(1):45. URL: <https://doi.org/10.1186/s13661-015-0303-y>. doi:10.1186/s13661-015-0303-y.
- [24] Campos J, Guerrero P, scar Snchez , Soler J. On the analysis of traveling waves to a nonlinear flux limited reactiondiffusion equation. *Ann I H Poincaré - NA* 2013;30(1):141 –55. URL: <http://www.sciencedirect.com/science/article/pii/S0294144912000637>. doi:<https://doi.org/10.1016/j.anihpc.2012.07.001>.
- [25] Campos J, Soler J. Qualitative behavior and traveling waves for flux-saturated porous media equations arising in optimal mass transportation. *Nonlinear Anal* 2016;137:266 –90. URL: <http://www.sciencedirect.com/science/article/pii/S0362546X1500437X>. doi:<https://doi.org/10.1016/j.na.2015.12.021>; nonlinear Partial Differential Equations, in honor of Juan Luis Vzquez for his 70th birthday.
- [26] Calvo J, Campos J, Caselles V, Sánchez O, Soler J. Flux-saturated porous media equations and applications. *EMS Surv Math Sci* 2015;2:131–218.
- [27] Calvo J, Campos J, Caselles V, Sánchez O, Soler J. Pattern formation in a flux limited reaction–diffusion equation of porous media type. *Invent Math* 2016;206(1):57–108. URL: <https://doi.org/10.1007/s00222-016-0649-5>. doi:10.1007/s00222-016-0649-5.

- [28] Calvo J. Singular traveling waves and non-linear reaction-diffusion equations. In: Computational Mathematics, Numerical Analysis and Applications. Springer; 2017, p. 189–94.
- [29] Calvo J. On sonic hedgehog morphogenic action and finite propagation speed models. *SeMA Journal* 2018;75(2):173–95. URL: <https://doi.org/10.1007/s40324-017-0128-y>. doi:10.1007/s40324-017-0128-y.
- [30] Garrione M, Sanchez L. Monotone traveling waves for reaction-diffusion equations involving the curvature operator. *Bound Value Probl* 2015;2015(1):45. URL: <https://doi.org/10.1186/s13661-015-0303-y>. doi:10.1186/s13661-015-0303-y.
- [31] Garduño FS, Maini P. An approximation to a sharp type solution of a density-dependent reaction-diffusion equation. *Appl Math Lett* 1994;7(1):47 – 51. URL: <http://www.sciencedirect.com/science/article/pii/0893965994900515>. doi:[http://dx.doi.org/10.1016/0893-9659\(94\)90051-5](http://dx.doi.org/10.1016/0893-9659(94)90051-5).
- [32] Ngamsaad W, Suantai S. Mechanically-driven spreading of bacterial populations. *Commun Nonlinear Sci Numer Simulat* 2016;35:88 – 96. URL: <http://www.sciencedirect.com/science/article/pii/S1007570415003718>. doi:<https://doi.org/10.1016/j.cnsns.2015.10.026>.
- [33] Newman W. Some exact solutions to a non-linear diffusion problem in population genetics and combustion. *J Theor Biol* 1980;85(2):325–34.
- [34] Eberl HJ, Demaret L. A finite difference scheme for a degenerated diffusion equation arising in microbial ecology. *Electron J Diff Eqns*, Conference 2007;15:77–95.
- [35] Press WH, Flannery BP, Teukolsky SA, Vetterling WT. *Numerical Recipes in C: The Art of Scientific Computing*. Cambridge University Press, Cambridge; 1988.
- [36] Arfken GB. *Mathematical Methods for Physicists*. Academic Press, San Diego; 1985.